Extended optical model analyses of elastic scattering and fusion cross sections for heavy-ion collisions with loosely bound projectiles at near-Coulomb-barrier energies

W. Y. So, S. W. Hong, and B. T. Kim
Department of Physics and Institute of Basic Science, Sungkyunkwan University, Suwon 440-746, Korea

T. Udagawa
Department of Physics, University of Texas, Austin, Texas 78712, USA
(Received 10 October 2003; published 9 June 2004)

Within the framework of an extended optical model, simultaneous χ^2 analyses are performed for elastic scattering and fusion cross-section data for ^{9}Be+^{209}Bi and ^{6}Li+^{208}Pb systems, both involving loosely bound projectiles, at near-Coulomb-barrier energies to determine the polarization potential as decomposed into direct reaction (DR) and fusion parts. We show that both DR and fusion potentials extracted from χ^2 analyses separately satisfy the dispersion relation, and that the expected threshold anomaly appears in the fusion part. The DR potential turns out to be a rather smooth function of the incident energy, and has a magnitude at the strong absorption radius much larger than the fusion potential, explaining why a threshold anomaly has not been seen in optical potentials deduced from fits to the elastic-scattering data without such a decomposition. Using the extracted DR potential, we examine the effects of projectile breakup on fusion cross sections σ_F. The observed suppression of σ_F in the above-barrier region can be explained in terms of the flux loss due to breakup. However, the observed enhancement of σ_F in the subbarrier region cannot be understood in terms of the breakup effect. Rather, the enhancement can be related to the Q value of the neutron transfer within the systems, supporting the ideas of Stelson *et al.* [Phys. Lett. B **205**, 190 (1988); Phys. Rev. C **41**, 1584 (1990)] that subbarrier fusion starts to occur when the colliding ions are at a distance where the barrier against the flow of the valence neutrons disappears and thus neutron exchange can take place freely.

DOI: 10.1103/PhysRevC.69.064606 PACS number(s): 24.10.−i, 25.70.Jj

I. INTRODUCTION

In our earlier publications [1–3], we proposed a unified approach to describe fusion within the framework of the direct reaction (DR) theory, the simplest of which was an extended optical model. There, we assumed an optical potential consisting of a volume-type fusion part, $U_F(r,E)$, and a surface-type DR part, $U_D(r,E)$, both being complex and energy dependent, together with the real Coulomb $V_C(r)$ and the bare (Hartree-Fock) nuclear potential $V_0(r)$. The total DR and fusion cross sections, σ_D and σ_F, respectively, were then calculated as an absorption cross section due to $U_D(r,E)$ and $U_F(r,E)$. In Refs. [2,3], using the extended optical model, we successfully carried out simultaneous χ^2 analyses of elastic scattering, total (sum of all different) direct reaction, and fusion cross-section data for heavy-ion collisions.

The original development [1] of the DR approach to fusion was motivated by questions concerning the radial distance at which fusion begins to occur. We called such a distance the fusion potential radius R_F, where $R_F=r_F(A_1^{1/3}+A_2^{1/3})$. An obvious question was raised when we recognized that there were two conflicting r_F values, i.e., the r_F value assumed in the barrier penetration model (BPM) [4,5] and the much larger r_F value implied in the DR theory. The BPM assumes that fusion occurs after two colliding ions pass through or go over the Coulomb barrier and approach each other within a critical distance $R_{cr}=r_{cr}(A_1^{1/3}+A_2^{1/3})$. The value of r_{cr} has customarily been assumed to be about 1.0 fm. Thus in the BPM, one has $r_F\approx r_{cr}\approx 1.0$ fm. However, in the DR theory, it is envisioned that fusion occurs once the colliding ions contact each other within the strong absorption radius [6] $R_{sa}=r_{sa}(A_1^{1/3}+A_2^{1/3})$. The value of r_{sa} is known to be about 1.5 fm. This means that $r_F\approx r_{sa}\approx 1.5$ fm. The r_F values assumed in the BPM and in the DR theory thus differ by about 50%.

Collisions between heavy ions are strongly dissipative, which means that once the ions start to interact and get excited, they go into states of more and more complex excitations, causing a strong damping of the relative kinetic energy between the two ions. Once this happens, the system can hardly go back to the elastic channel. The large r_F value implied in the DR theory reflects this highly dissipative nature of the collisions. The approach of Ref. [1] was developed to describe fusion in a way consistent with this picture. It is worth emphasizing here that the success of the distorted-wave Born approximation (DWBA) in dealing with DR is due to the strong absorption of the distorted waves inside R_{sa}, so that the reaction can take place only in the peripheral region, where the interaction between the two colliding ions is effectively weak. Thus one can treat the interaction by means of the Born approximation.

In a more recent publication [7], we extended the optical model approach of Refs. [2,3] to permit evaluation of the angular distribution of the total DR. This has enabled us to integrate the angular distribution data during the analyses. The method has been applied to ^{16}O+^{208}Pb [7] and ^{6}He +^{209}Bi [8] systems at incident energies near the Coulomb-barrier height.

In Ref. [8], the ^{6}He+^{209}Bi system was considered as an example of collisions involving loosely bound projectiles,

which has been extensively studied recently. There are two important questions raised in these studies: One concerns the so-called threshold anomaly [9,10] (rapid energy variation in the strength of the optical potential), and the other concerns the effect of a high probability of breakup on the fusion cross section, σ_F. Thus data have been taken not only for elastic scattering but also for fusion and breakup in collisions induced by such loosely bound projectiles, e.g., ^{6}He [11–13], ^{6}Li [14–20], and ^{9}Be [21–25,27,28]. As expected, large α production (breakup) cross sections have been observed in these collisions [13,15–18,25–28].

These data have shown that the threshold anomaly almost always seen for tightly bound projectiles is absent for such loosely bound projectiles. The absence of the threshold anomaly has often been ascribed to the large probability of breakup of these loosely bound projectiles [9]. The experimental fusion cross sections are strongly suppressed at energies above the Coulomb barrier, while they are in some cases enhanced at subbarrier energies, particularly for ^{6}He + ^{209}Bi [11].

It was pointed out some time ago [29] that the threshold anomaly was due to fusion, specifically to the coupling of the elastic channel with fusion channels. In the case where fusion dominates the reaction, the threshold anomaly naturally manifests itself in the optical potentials extracted from the analyses of elastic scattering data. However, in the case where breakup (or DR in general) dominates, the energy dependence of the resultant optical potentials is governed by DR and thus is quite smooth [9]. One can thus expect that a rapid variation would not appear in the potential when a process is dominated by DR. In order to see the threshold anomaly in such cases, it is thus necessary to separate the potential into fusion and DR (breakup) parts. The optical model approach used in Refs. [1–3] is a possible way to achieve such a separation. In Ref. [8], by using such an approach, simultaneous χ^2 analyses were performed on the data for the elastic scattering, breakup, and fusion for ^{6}He + ^{209}Bi, and a clean separation of the fusion potential from the DR portion was achieved. It was shown that a threshold anomaly appeared in the fusion potential as expected. At the same time, it was possible to explain the suppression of the fusion cross section at above-barrier energies as a result of large breakup.

The aim of the present study is to extend this type of analysis to the ^{6}Li + ^{208}Pb and ^{9}Be + ^{209}Bi systems, both involving loosely bound projectiles. In making such an extension, however, we encounter the difficulty that no reliable total DR cross-section data are available. For these systems the α production cross sections have been measured [15–18,25–28], but the results are still controversial. (After writing the paper we came across Ref. [28], where the experimental total DR cross sections were reported for the ^{9}Be + ^{209}Pb system. We will mention these data in Secs. III and IV D) Also, there is no guarantee that the measured breakup (α production) cross section exhausts the total DR cross section, so that one can use the breakup cross section as σ_D^{exp}. In the present study, we thus generate first the semiexperimental total reaction cross section, $\sigma_R^{semi\text{-}exp}$ from the measured elastic scattering cross section, $d\sigma_E^{exp}/d\Omega$. Such an approach to generate $\sigma_R^{semi\text{-}exp}$ from $d\sigma_E^{exp}/d\Omega$ has been proposed and tested, e.g., in Refs. [6,30–33]. In Sec. II, we first discuss characteristic features of elastic and breakup cross-section data considered in the present study. In Sec. III, details of the method of generating $\sigma_R^{semi\text{-}exp}$ are explained. Using $\sigma_R^{semi\text{-}exp}$, we further generate a semiexperimental total DR cross section, $\sigma_D^{semi\text{-}exp}$, as $\sigma_D^{semi\text{-}exp} = \sigma_R^{semi\text{-}exp} - \sigma_F^{exp}$, which will be used as σ_D^{exp}. Simultaneous χ^2 analyses of the data of $d\sigma_E^{exp}/d\Omega$, σ_F^{exp}, and $\sigma_D^{semi\text{-}exp}$ are then carried out as discussed in Sec. IV, which presents details of the analysis method. In Sec. V, the results are summarized and discussed with an emphasis on two important issues, i.e., the threshold anomaly and the breakup effects on fusion. Finally, Sec. VI concludes the paper.

II. REVIEW OF EXPERIMENTAL DATA

We begin by discussing some of the characteristic features of elastic scattering and DR data for the ^{6}Li + ^{208}Pb and ^{9}Be + ^{209}Bi systems considered in this study, in comparison with those for ^{6}He + ^{209}Bi studied previously and discussed in Ref. [8]. As remarked there, unusual features of collisions with loosely bound projectiles can best be seen in the ratio P_i, defined by

$$P_i \equiv \frac{d\sigma_i}{d\Omega} \Big/ \frac{d\sigma_C}{d\Omega} = d\sigma_i/d\sigma_C \quad (i = E \text{ or } D), \tag{1}$$

as a function of the distance of the closest approach D (or the reduced distance d) [6,30,34], where D is related to the scattering angle θ by

$$D = d(A_1^{1/3} + A_2^{1/3}) = \frac{1}{2} D_0 \left(1 + \frac{1}{\sin(\theta/2)} \right) \tag{2}$$

with

$$D_0 = \frac{Z_1 Z_2 e^2}{E},$$

and D_0 is the distance of the closest approach in a head-on collision (s wave). Here (A_1, Z_1) and (A_2, Z_2) are the mass and charge of the projectile and target ions, respectively, and E is the incident energy in the center-of-mass system. P_E and P_D as defined by Eq. (1) are referred to as the elastic and DR probabilities, respectively.

In Figs. 1 and 2, we present experimental values of P_E and P_D for all available incident energies as a function of the reduced distance d for ^{6}Li + ^{208}Pb and ^{9}Be + ^{209}Bi, respectively. Note that P_D in Fig. 1(b) is that for the α-singles cross section and does not include cross sections of, e.g., deuteron production that may come from breakup followed by absorption of an α by the target nucleus (incomplete fusion). There is experimental evidence [19] that such incomplete fusion events give rise to a significant contribution to P_D. This means that P_D shown in Fig. 1(b) may be underestimated by a certain factor. In Fig. 2, plotted are the P_E values only, since for ^{9}Be + ^{209}Bi the angular distribution data needed for P_D are not available.

As seen in Figs. 1(a) and 2, the values of P_E at different incident energies line up to form a very narrow band. This is a characteristic feature seen in heavy-ion collisions [7], irrespective of whether the projectile is tightly bound or not,

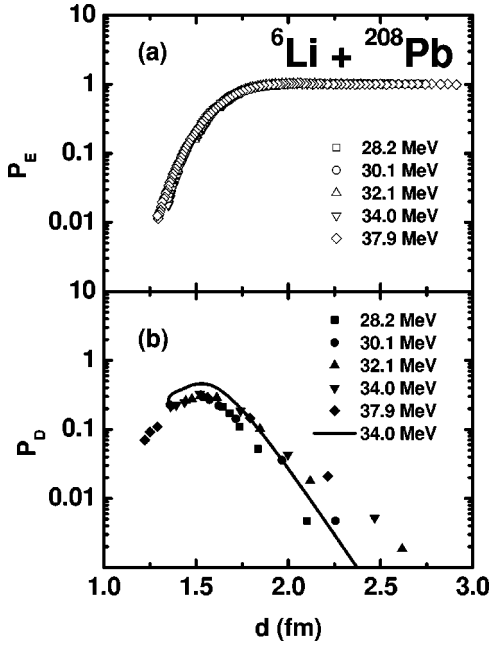

FIG. 1. The experimental (a) elastic and (b) DR probabilities, P_E and P_D, respectively, as functions of the reduced distance d for the ^{6}Li+^{208}Pb system at $E_{\text{c.m.}}=28.2$, 30.1, 32.1, 34.0, and 37.9 MeV. The data are taken from Refs. [14,18]. The solid curve plotted in the lower panel is our theoretical prediction (see details in the discussion in Sec. IV C). The experimental errors in P_E and P_D are less than 10% and 1%, respectively.

reflecting the semiclassical nature of these collisions. P_E remains close to unity until the two ions approach each other within a distance d_I, where P_E begins to fall off. The distance d_I is usually called the interaction distance, at which the nuclear interactions between the colliding ions are switched on, so to speak. The values of d_I are about 1.9 fm for ^{6}Li +^{208}Pb and 1.8 fm for ^{9}Be+^{209}Bi. Note that the corresponding value for ^{6}He+^{209}Bi is 2.2 fm [8]. These values for loosely bound projectiles are significantly larger than those ($d_I \approx 1.68$ fm) for tightly bound projectiles [6,7,30,34].

As demonstrated [34] for tightly bound projectiles, P_E falls off approximately exponentially (linearly in the logarithmic scale) for $d < d_I$. This is, however, not the case for loosely bound projectiles as seen in Figs. 1 and 2. In the region just inside of d_I, P_E falls off roughly quadratically in the logarithmic scale. This is also the case for ^{6}He+^{209}Bi [8]. Thus, the existence of the quadratic falloff region just inside d_I seems to be another characteristic feature of P_E for loosely bound projectiles.

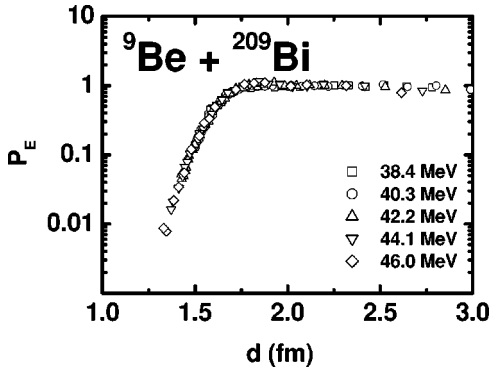

FIG. 2. The experimental elastic probability, P_E, as a function of the reduced distance d for the ^{9}Be+^{209}Bi system at $E_{\text{c.m.}}=38.4$, 40.3, 42.2, 44.1, and 46.0 MeV. The data are taken from Ref. [23]. The errors in P_E are less than 16%.

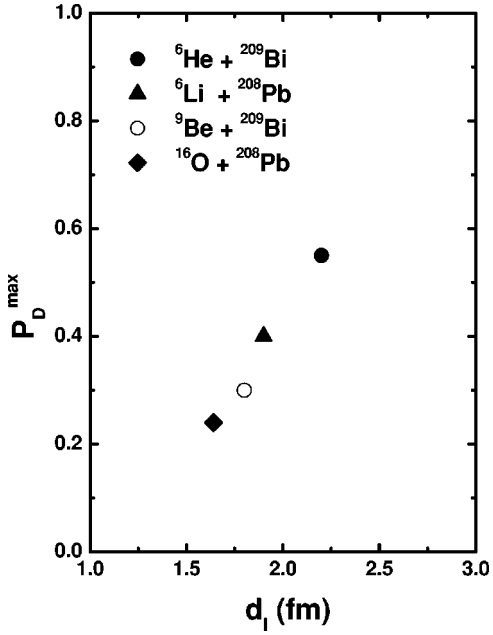

FIG. 3. The maximum values of DR probability $P_D(P_D^{max})$ are plotted against the interaction radius d_I extracted from P_E. For ^{6}He+^{209}Bi, Fig. 1 of Ref. [8] is used to extract P_D^{max}. P_D^{max} for ^{6}Li+^{208}Pb is obtained by adding the breakup contribution [the maximum P_D in Fig. 1(b)] to the incomplete fusion contribution (about 30% from Fig. 3 of Ref. [19]). This sum agrees with the maximum value of our predicted P_D (solid curve) in Fig. 1(b). For ^{9}Be+^{209}Bi, P_D^{max} is obtained by summing breakup, transfer, and Coulomb excitation contributions at 12.5 fm in Fig. 3 of Ref. [27], and the incomplete fusion contribution (about 20% from Fig. 2 of Ref. [22]). For ^{16}O+^{208}Pb, Fig. 1 of Ref. [7] is used to extract P_D^{max}.

We may ascribe these features to breakup, or more generally to DR; in fact the d_I values are strongly correlated with the magnitudes of the total DR cross sections. This is shown in Fig. 3, where the maximum values of $P_D(P_D^{max})$ that presumably measure the strength of DR are plotted against d_I. As seen, P_D^{max} increases approximately linearly with d_I (DR cross sections tend to be larger for systems with larger d_I). Furthermore, as can be seen in Fig. 1, if one adds P_D to P_E, the sum P_E+P_D comes very close to unity in the region of the quadratic falloff (more so, if one takes into consideration the incomplete fusion contribution to P_D remarked above), implying that the falloff of P_E from unity in the quadratic region is primarily due to breakup (DR). The same feature was also observed for ^{6}He+^{209}Bi (see Fig. 1 of Ref. [8]). From what has been discussed so far, we may safely conclude that the d_I value can be used as a measure of the importance of the breakup (DR) effect. Along this line of reasoning, since d_I for ^{6}He, ^{6}Li, and ^{9}Be are about 2.2, 1.9, and 1.8 fm, respectively, ^{6}He is the most characteristic

loosely bound projectile (in fact a well-known halo nucleus), ^{6}Li is the next, and ^{9}Be is the least among these three under consideration.

The experimental data of P_D will be used for fixing the values of the geometrical parameters r_D and a_D for the DR potential. This point [together with the nature of the solid line shown in Fig. 1(b)] will be discussed again later in Sec. IV.

III. EXTRACTING SEMIEXPERIMENTAL DR CROSS SECTION

It has been suggested [6,30–33] that in heavy-ion collisions the total reaction cross section σ_R can be extracted from the measured elastic scattering cross section $d\sigma_E/d\Omega$ as

$$\sigma_R = \sigma_C - \sigma_E, \tag{3}$$

where σ_C and σ_E are the angle-integrated total Rutherford and elastic scattering cross sections, respectively,

$$\sigma_i = \int \frac{d\sigma_i}{d\Omega} d\Omega \quad (i = C \text{ or } E). \tag{4}$$

Equation (3) is based on the optical theorem for charged particles [6], which reads

$$\sigma_R = \sigma_C - \sigma_E + \Delta\sigma, \tag{5}$$

where $\Delta\sigma$, the correction term, is given in terms of the nuclear part of the forward scattering amplitude, $f^N(\theta=0)$, as

$$\Delta\sigma = \frac{4\pi}{k} \mathrm{Im}[f^N(\theta=0)]. \tag{6}$$

For heavy-ion collisions, $\Delta\sigma$ is generally small, justifying the use of Eq. (3) for generating σ_R. We refer to σ_R calculated by Eq. (3) as a semiexperimental reaction cross section, $\sigma_R^{semi\text{-}exp}$. Once $\sigma_R^{semi\text{-}exp}$ is extracted, and if the experimental fusion cross section, σ_F^{exp}, is available, one can further generate a semiexperimental total DR cross section, $\sigma_D^{semi\text{-}exp}$, as

$$\sigma_D^{semi\text{-}exp} = \sigma_R^{semi\text{-}exp} - \sigma_F^{exp}. \tag{7}$$

Unfortunately, it is usually difficult to use this method of generating $\sigma_R^{semi\text{-}exp}$ as described above. The reason is that, besides the well-known difficulty of measuring $d\sigma_E/d\Omega$ at forward angles, data for $d\sigma_E^{exp}/d\Omega$ are usually available only over a limited range of angles, which makes it difficult to obtain a reliable value of the angle-integrated σ_E. We thus resort here to the empirical fact [35] that the total reaction cross section calculated from the optical model fit to the available elastic scattering cross section data, $d\sigma_E^{exp}/d\Omega$, usually agrees well with the experimental σ_R, in spite of the well known ambiguities of the optical potential. This means that we may replace $\sigma_C - \sigma_E$ in Eq. (3) by the total reaction cross section calculated from the optical model fit to available $d\sigma_E^{exp}/d\Omega$. This approach seems to work even for loosely bound projectiles, as demonstrated recently by Kolata *et al.* in the ^{6}He case [11].

In this study, we thus first carry out rather simple optical model χ^2 analyses of elastic scattering data for the ^{6}Li $+^{208}$Pb and ^{9}Be$+^{209}$Bi systems. For these preliminary analyses, we assume the optical potential to be a simple sum of two volume-type potentials $V_0(r)$ and $U_1(r,E)$, where $V_0(r)$ is the real, energy-independent bare potential [the same bare potential will be used in Eq. (9) later for the full χ^2 analyses], while $U_1(r,E)$ is a complex potential with common geometrical parameters for both real and imaginary parts. The elastic scattering data are then fitted with a fixed radius parameter r_1 for $U_1(r,E)$ but with all three other parameters varied, the real and the imaginary strengths V_1 and W_1, and the diffuseness parameter a_1. The χ^2 fitting is done for three choices of the radius parameter: $r_1 = 1.3$, 1.4, and 1.5 fm. These different choices of the r_1 value are made in order to examine the dependence of the resulting $\sigma_R^{semi\text{-}exp}$ on the choice of the parameters.

The values of $\sigma_R^{semi\text{-}exp}$ thus extracted are summarized in Table I, where the values of $\Delta\sigma$ estimated from these preliminary optical model calculations are also shown. (The optical potential parameters from these preliminary calculations are not listed here for brevity.) The $\sigma_R^{semi\text{-}exp}$ values calculated in Refs. [14] and [23] for ^{6}Li$+^{208}$Pb and ^{9}Be$+^{209}$Bi, respectively, are also listed in the last column. As seen in Table I, the estimated $\Delta\sigma$ values are rather small compared with $\sigma_R^{semi\text{-}exp}$, justifying the use of Eq. (3). Also, the mean-square deviations of $\sigma_R^{semi\text{-}exp}$ obtained by the use of different r_1 values are rather small. Further, $\sigma_R^{semi\text{-}exp}$ as determined in Refs. [14] and [23] using optical potential parameters quite different from those used above, agree with ours within 10%, suggesting that this method can yield $\sigma_R^{semi\text{-}exp}$ without much ambiguity.

Using $\sigma_R^{semi\text{-}exp}$ extracted in this way, we generate $\sigma_D^{semi\text{-}exp}$ by employing Eq. (7). For the case of ^{6}Li$+^{208}$Pb, $\sigma_D^{semi\text{-}exp}$ thus generated are found to be 10%–30% larger than the experimental total breakup cross section measured by Signorini *et al.* [18], which seems to be reasonable; the difference may be due to the incomplete fusion events mentioned in Sec. II. For the ^{9}Be$+^{209}$Bi case, extracted $\sigma_D^{semi\text{-}exp}$ are somewhat larger than the observed breakup cross section reported in Ref. [16], but close to the values reported in Ref. [27]. Also, the sum of the DR cross section measured for ^{9}Be $+^{208}$Pb [28] agrees well with our $\sigma_D^{semi\text{-}exp}$ as will be seen later in Fig. 8.

IV. SIMULTANEOUS χ^2 ANALYSES

Simultaneous χ^2 analyses were performed on the data for $d\sigma_E^{exp}/d\Omega$, σ_F^{exp}, and $\sigma_D^{semi\text{-}exp}$ for the ^{6}Li$+^{208}$Pb and ^{9}Be $+^{209}$Bi systems; $\sigma_D^{semi\text{-}exp}$ are generated from $d\sigma_E^{exp}/d\Omega$ as described in the previous section. $d\sigma_E^{exp}/d\Omega$ and σ_F^{exp} are taken from the literature [14,19,21,23]. Since σ_F^{exp} data for ^{6}Li$+^{208}$Pb were not available at the time the analyses were carried out, use was made of data taken for ^{6}Li$+^{209}$Bi [19]. After finishing the analyses, we received data taken for ^{6}Li $+^{208}$Pb [20]. But since the new data are found to be essentially the same as the data used, no attempt has been made to repeat the calculations using the new data.

A. Necessary formulas

The optical potential $U(r,E)$ that we use in the present study has the following form:

TABLE I. $\sigma_R^{semi\text{-}exp}$ (in mb) extracted from Eq. (3) is compared with other values of $\sigma_R^{semi\text{-}exp}$. In this table $\sigma_R^{semi\text{-}exp}$ is shortened as σ_R for simplicity.

		r_1							
	E_{lab}	1.3 fm		1.4 fm		1.5 fm			
System	(MeV)	σ_R	$\Delta\sigma$	σ_R	$\Delta\sigma$	σ_R	$\Delta\sigma$	Average	Others[a]
^{6}Li+^{208}Pb	29	222	0.0	221	0.0	221	0.0	221	228
	31	395	0.0	394	0.0	393	0.0	394	431
	33	625	−0.1	624	−0.1	621	0.0	623	666
	35	865	−0.3	850	−0.4	824	−0.6	846	897
	39	1293	0.2	1278	−0.1	1237	−1.0	1269	1303
^{9}Be+^{209}Bi	40	256	0.0	256	0.0	253	0.0	255	281
	42	451	0.0	449	0.0	444	0.0	448	463
	44	612	−0.1	611	−0.1	616	−0.1	613	601
	46	771	2.6	766	−1.3	774	0.0	770	766
	48	929	−0.4	919	1.0	931	−0.6	926	950

[a] $\sigma_R^{semi\text{-}exp}$ for ^{6}Li+^{208}Pb are taken from Ref. [14], while $\sigma_R^{semi\text{-}exp}$ for ^{9}Be+^{209}Bi are calculated by using the optical potential parameters deduced in Ref. [23].

$$U(r) = V_C(r) - [V_0(r) + U_F(r;E) + U_D(r;E)], \tag{8}$$

where $V_C(r)$ is the usual Coulomb potential with $r_C = 1.25$ fm, and $V_0(r)$ is the bare (Hartree-Fock) nuclear potential. $U_F(r;E)$ and $U_D(r;E)$ are, respectively, fusion and DR parts of the so-called polarization potential [36] that originates from couplings to the respective reaction channels. Both $U_F(r;E)$ and $U_D(r;E)$ are complex and their forms are assumed to be of volume-type and surface-derivative-type [7], respectively. Explicitly, $V_0(r)$, $U_F(r;E)$, and $U_D(r;E)$ are given by

$$V_0(r) = V_0 f(X_0), \tag{9}$$

$$U_F(r;E) = [V_F(E) + iW_F(E)] f(X_F), \tag{10}$$

and

$$U_D(r;E) = [V_D(E) + iW_D(E)] 4a_D \frac{df(X_D)}{dR_D}, \tag{11}$$

where $f(X_i) = [1+\exp(X_i)]^{-1}$ with $X_i = (r-R_i)/a_i$ ($i = 0$, D, and F) is the usual Woods-Saxon function, while $V_F(E)$, $V_D(E)$, $W_F(E)$, and $W_D(E)$ are the energy-dependent strength parameters. We assume the geometrical parameters of the real and imaginary potentials to be the same, and thus the strength parameters $V_i(E)$ and $W_i(E)$ ($i=F$ or D) are related through a dispersion relation [9],

$$V_i(E) = V_i(E_s) + \frac{E-E_s}{\pi} \mathrm{P} \int_0^\infty dE' \frac{W_i(E')}{(E'-E_s)(E'-E)}, \tag{12}$$

where P stands for the principal value and $V_i(E_s)$ is the value of $V_i(E)$ at a reference energy $E=E_s$. Later, we will use Eq. (12) to generate the final real strength parameters $V_F(E)$ and $V_D(E)$, after $W_F(E)$ and $W_D(E)$ are fixed from χ^2 analyses. Note that the breakup cross section may include contributions from both Coulomb and nuclear interactions, which imply that the direct reaction potential includes effects coming not only from the nuclear interaction, but also from the Coulomb interaction.

$V_0(r)$ in Eq. (9) may also have an energy dependence coming from the nonlocality due to the knockon-exchange contribution. We ignore such effects as they are expected to be small for heavy-ion scattering [6], and employ the real potential parameters used in Ref. [33] assuming that all the unusual features of the potential may be put into the polarization parts, particularly the DR part. The parameters used are $V_0 = 18.36$ MeV, $r_0 = 1.22$ fm, and $a_0 = 0.57$ fm for ^{6}Li +^{208}Pb and $V_0 = 23.02$ MeV, $r_0 = 1.22$ fm, and $a_0 = 0.57$ fm for ^{9}Be+^{209}Bi [33]. Note that these potentials are shallow, which is often required in fitting elastic scattering data of such projectiles as ^{6}Li and ^{9}Be [37].

In performing the optical model calculation, one can evaluate σ_F and σ_D by using the following expression [1–3,38]

$$\sigma_i = \frac{2}{\hbar v} \langle \chi^{(+)} | W_i(r) | \chi^{(+)} \rangle \quad (i = F \text{ or } D), \tag{13}$$

where $\chi^{(+)}$ is the usual distorted wave function that satisfies the Schrödinger equation with the full optical model potential $U(r,E)$ in Eq. (8). σ_F and σ_D are thus calculated within the same framework as $d\sigma_E/d\Omega$. Such a unified description enables us to treat all the different types of reactions on the same footing.

In Ref. [7], we proposed using the following expression:

$$P_D \approx T_{D;\ell} = \frac{8}{\hbar v} \int_0^\infty |\chi_\ell(r)|^2 W_D(r) dr, \tag{14}$$

which is derived using the semiclassical nature of heavy-ion collisions. The above relation may be used to analyze angular distribution data, and particularly to fix the shape parameters for the DR potential, r_D and a_D involved in $f(X_D)$, since

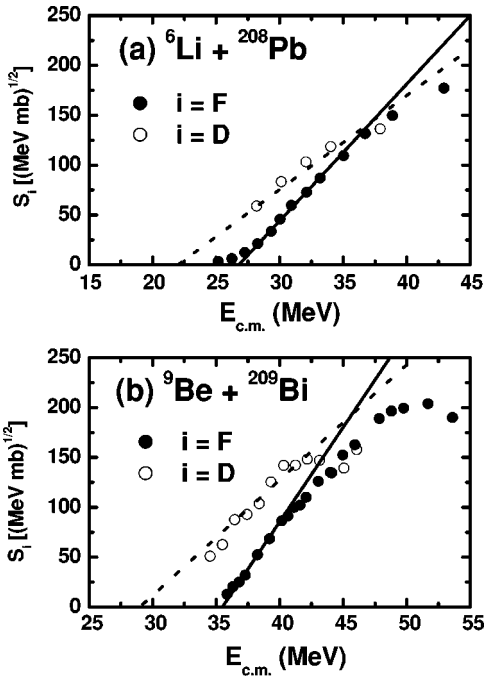

FIG. 4. The Stelson plot of $S_i=\sqrt{E_{\mathrm{c.m.}}\sigma_i}$ for DR ($i=D$, open circles) and fusion ($i=F$, solid circles) cross sections for (a) ^{6}Li $+^{208}$Pb and (b) ^{9}Be$+^{209}$Bi systems. The straight lines are drawn to show the extraction of the threshold energies $E_{0,i}$.

P_D is sensitive to these parameters. In Sec. IV C we shall discuss the use of Eq. (14) to fix the values of the parameters.

B. Threshold energies of subbarrier fusion and DR

In the present study, we utilize as an important ingredient the so-called threshold energies $E_{0,F}$ and $E_{0,D}$ of subbarrier fusion and DR, respectively, which are defined as zero intercepts of the linear representation of the quantities $S_i(E)$, defined by

$$S_i \equiv \sqrt{E\sigma_i} \approx \alpha_i(E-E_{0,i}) \quad (i=D \text{ or } F), \tag{15}$$

where α_i is a constant. S_i with $i=F$, i.e., S_F is the quantity introduced originally by Stelson *et al.* [39], who showed that in the subbarrier region S_F from the measured σ_F can be represented very well by a linear function of E (linear systematics) as in Eq. (15). In Ref. [7], we extended linear systematics to DR cross sections; in fact, the DR data are also well represented by a linear function.

In Fig. 4 we present the experimental $S_F(E)$ and $S_D(E)$ results for both ^{6}Li$+^{208}$Pb and ^{9}Be$+^{209}$Bi. From the zeros of $S_i(E)$, one can extract the $E_{0,i}$ values; $E_{0,D}=22.0$ MeV and $E_{0,F}=26.8$ MeV for ^{6}Li$+^{208}$Pb, as well as $E_{0,D}=29.0$ MeV and $E_{0,F}=35.5$ MeV for ^{9}Be$+^{209}$Bi. In both cases, the observed S_i are very well approximated by straight lines and thus $E_{0,i}$ can be extracted without much ambiguity.

$E_{0,i}$ may then be used as the energy where the imaginary potential $W_i(E)$ becomes zero, i.e., $W_i(E_{0,i})=0$ [7,8]. This procedure will be used later in obtaining a mathematical expression for $W_i(E)$.

TABLE II. Geometrical parameters used in the χ^2 analyses.

	^{6}Li$+^{208}$Pb	^{9}Be$+^{209}$Bi
r_F(fm)	1.40	1.40
a_F(fm)	0.42	0.32
r_D(fm)	1.47	1.51
a_D(fm)	0.85	0.72

C. χ^2 analyses

All χ^2 analyses in the present work were carried out by using $V_0(r)$ as given in Sec. IV A and by using the fixed geometrial parameters for the polarization potentials. The fixed shape parameters are listed in Table II. These values are obtained by making some preliminary analyses, starting with $r_F=1.40$ fm, $a_F=0.40$ fm, $r_D=1.58$ fm, and $a_D=0.85$ fm, which are the averages of each parameter determined in our previous studies [7,8]. In fixing the r_D and a_D values for ^{6}Li$+^{208}$Pb, the experimental P_D was fitted by using Eq. (14). In Fig. 1(b), we show as an example (solid curve) P_D as calculated for $E_{\mathrm{c.m.}}=34.0$ MeV in the course of these preliminary calculations. It is remarkable that the elastic scattering and the DR data require large diffuseness parameters of $a_D=0.85$ and 0.72 fm for ^{6}Li$+^{208}$Pb and ^{9}Be$+^{209}$Bi, respectively. These values are much larger than that ($a_D=0.45$ fm) for a typical tightly bound projectile, such as ^{16}O [7], and reflect the large d_I values for these systems.

With the geometrical parameters in Table II the χ^2 analyses then proceeded in two steps: in the first step, all four strength parameters, $V_D(E)$, $W_D(E)$, $V_F(E)$, and $W_F(E)$ were varied. In this step, we were able to fix nicely the strength parameters of the DR potential, $V_D(E)$ and $W_D(E)$, in the sense that $V_D(E)$ and $W_D(E)$ were determined as smooth functions of E. The values of $V_D(E)$ and $W_D(E)$ thus extracted are presented in Figs. 5 and 6 by open circles. It is remarkable that the resultant $W_D(E)$ can be well represented by the following function of $E(=E_{\mathrm{c.m.}})$ (in units of MeV):

$$W_D(E)=\begin{cases} 0 & \text{for } E \leqslant E_{0,D}=22.0 \\ 0.083(E-22.0) & \text{for } 22.0<E\leqslant 28.0 \\ 0.023(E-28.0)+0.50 & \text{for } 28.0<E\leqslant 37.9 \\ 0.73 & \text{for } 37.9<E \end{cases} \tag{16}$$

for the ^{6}Li$+^{208}$Pb system and

$$W_D(E)=\begin{cases} 0 & \text{for } E \leqslant E_{0,D}=29.0 \\ 0.026(E-29.0) & \text{for } 29.0<E\leqslant 40.0 \\ 0.29 & \text{for } 40.0<E \end{cases} \tag{17}$$

for the ^{9}Be$+^{209}$Bi system. Note that the threshold energy where $W_D(E)$ becomes zero is set equal to $E_{0,D}$ as determined in the preceding section. The dotted lines in the lower panels of Figs. 5 and 6 represent Eqs. (16) and (17). The dotted lines in the upper panels of Figs. 5 and 6 denote V_D as predicted by the dispersion relation Eq. (12), with $W_D(E)$ given by Eqs. (16) and (17), respectively. As seen, the dotted

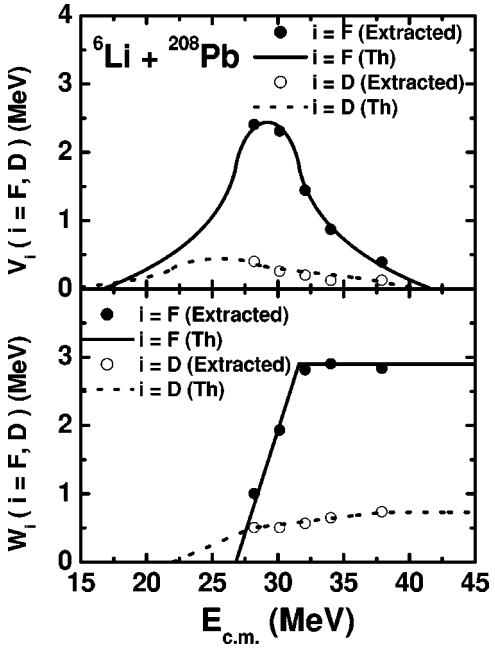

FIG. 5. The strength parameters V_i (upper panel) and W_i (lower panel) for $i=D$ and F as functions of $E_{\mathrm{c.m.}}$ for the ^{6}Li+^{208}Pb system. The open and solid circles are the values for $i=D$ and F, respectively. The lines in the lower panel denote W_D and W_F from Eqs. (16) and (18), respectively, while the curves in the upper panel represent V_D and V_F calculated by using the dispersion relation Eq. (12) with W_i given by Eqs. (16) and (18).

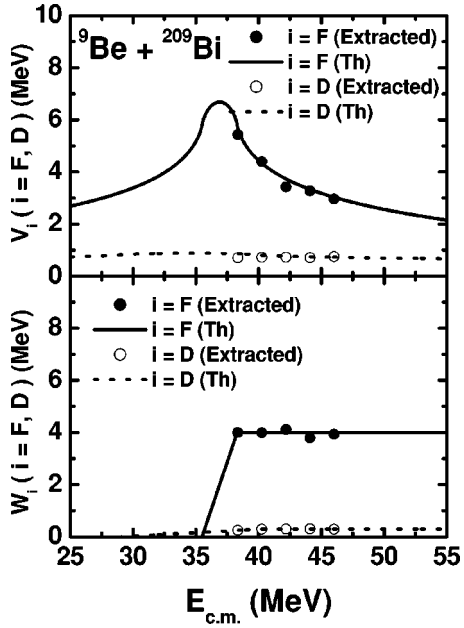

FIG. 6. The same as in Fig. 5, but for the ^{9}Be+^{209}Bi system. The solid (dotted) line in the lower panel denotes W_F (W_D) from Eq. (19) [Eq. (17)]. The solid (dotted) curve in the upper panel represents V_F (V_D) obtained by the dispersion relation.

lines reproduce the open circles very well, indicating that $V_D(E)$ and $W_D(E)$ extracted by the χ^2 analyses satisfy the dispersion relation well.

In the first χ^2 fit, however, the values of $V_F(E)$ and $W_F(E)$ could not be reliably fixed in the sense that the values extracted fluctuated considerably as functions of E. This is understandable from the expectation that the elastic scattering data can probe most accurately the optical potential in the peripheral region, which is nothing but the region characterized by the DR potential. The part of the nuclear potential responsible for fusion is thus difficult to pin down in such a way.

In order to obtain more reliable information on V_F and W_F, we thus performed the second step of the χ^2 analysis; this time, instead of doing a four-parameter search, we fixed V_D and W_D as determined by the first χ^2 fitting, i.e., $W_D(E)$ given by Eqs. (16) and (17) and $V_D(E)$ as given by the dispersion relation. We then performed a two-parameter χ^2 analyses, treating only $V_F(E)$ and $W_F(E)$ as adjustable parameters. The values thus determined are presented in Figs. 5 and 6 by solid circles. As seen, $V_F(E)$ and $W_F(E)$ are found in this way to be smooth functions of E. $W_F(E)$ can be well represented by

$$W_F(E)=\begin{cases}0 & \text{for } E\leqslant E_{0,F}=26.8\\ 0.403(E-26.8) & \text{for } 26.8<E\leqslant 34.0\\ 2.90 & \text{for } 34.0<E\end{cases} \quad (18)$$

for the ^{6}Li+^{208}Pb system and

$$W_F(E)=\begin{cases}0 & \text{for } E\leqslant E_{0,F}=35.5\\ 1.60(E-35.5) & \text{for } 35.5<E\leqslant 38.0\\ 4.00 & \text{for } 38.0<E\end{cases} \quad (19)$$

for the ^{9}Be+^{209}Bi system. As in the case for $W_D(E)$, the threshold energy where $W_F(E)$ becomes zero is set equal to $E_{0,F}$. The solid lines in the lower panels of Figs. 5 and 6 represent $W_F(E)$ in Eqs. (18) and (19). Using $W_F(E)$ given by these equations, one can generate $V_F(E)$ from the dispersion relation. The results are shown by the solid curves in the upper panels of Figs. 5 and 6, which again reproduce the extracted solid circles well. This means that the fusion potential determined from the present analysis also satisfies the dispersion relation.

D. Final calculated cross sections and comparison with the data

Using $W_D(E)$ given by Eqs. (16) and (17), and $W_F(E)$ given by Eqs. (18) and (19), together with $V_D(E)$ and $V_F(E)$ generated by the dispersion relation, we performed the final calculations of the elastic, DR, and fusion cross sections. The results are presented in Figs. 7 and 8 in comparison with the experimental data. All the data are well reproduced by the calculations. We remark that the sum of the DR cross sections for ^{9}Be+^{208}Pb [28] plotted by the squares in Fig. 8(b) agree well with our $\sigma_D^{semi\text{-}exp}$ denoted by the open circles. The final calculated cross sections obtained by employing $V_i(E)$ from the dispersion relation are found to be essentially the same as those obtained by the second χ^2 analyses.

In the next section, we shall present discussions of the results of the present analyses, with an emphasis on the

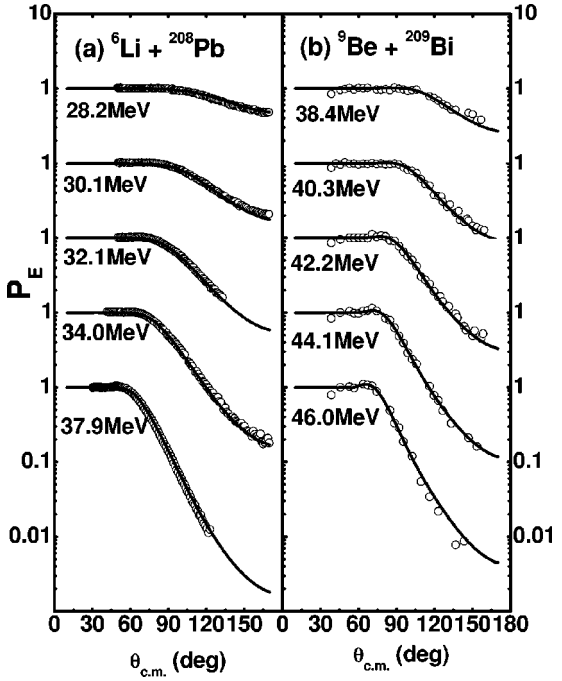

FIG. 7. Ratios of the elastic scattering cross sections to the Rutherford cross section calculated with our final dispersive optical potential for (a) ^{6}Li+^{208}Pb and (b) ^{9}Be+^{209}Bi systems are shown in comparison with the experimental data. The data are taken from Refs. [14,23].

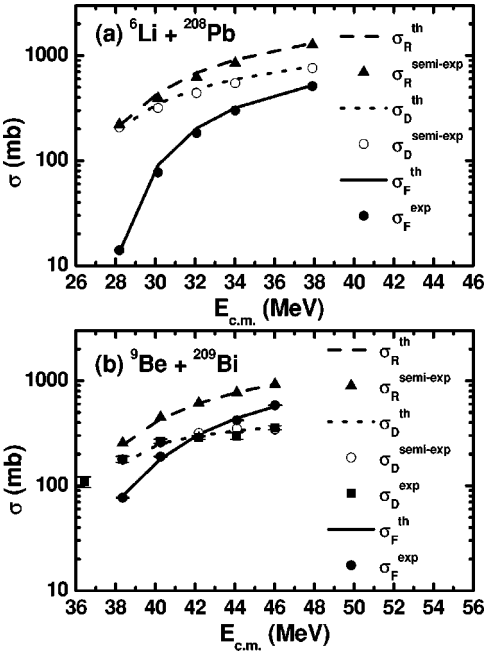

FIG. 8. DR and fusion cross sections calculated with our final dispersive optical potential for (a) ^{6}Li+^{208}Pb and (b) ^{9}Be+^{209}Bi systems are shown in comparison with the experimental data. $\sigma_D^{semi\text{-}exp}$, denoted by the open circles, are as described in Sec. II. σ_D^{exp} denoted by the solid squares for ^{9}Be+^{209}Bi are actually from the experimental DR cross sections for ^{9}Be+^{208}Pb [28]. The fusion data are from Refs. [19,21]. Note that the data of Ref. [19] are not for the ^{6}Li+^{208}Pb, but for ^{6}Li+^{209}Bi. (See the text for the details.) The errors in σ_F^{exp} are less than 10%.

threshold anomaly and the effect of the breakup on σ_F. A brief discussion will also be given on the effects of the DR and fusion potentials on the elastic scattering cross section.

V. DISCUSSIONS

A. Threshold anomaly

Since we have succeeded in decomposing the polarization potential into fusion and DR parts, it is now possible to examine their energy dependence separately: As seen in Figs. 5 and 6, the strength parameters $V_F(E)$ and $W_F(E)$ of the fusion potential show strong variations as functions of energy around the Coulomb-barrier energies, while that is not the case for the DR potential strengths $V_D(E)$ and $W_D(E)$. They are rather smooth functions of E. Similar results have already been seen for the ^{6}He+^{209}Bi system [8].

Because the radial shapes of the fusion and DR potentials are different from each other, the magnitudes of the strength parameters alone cannot provide information on the relative importance of the two potentials. It may best be seen by comparing the values of these potentials at the strong absorption radius R_{sa}; $V_i(R_{sa};E)$ and $W_i(R_{sa};E)$. These values are plotted in Fig. 9 as a function of $E_{\text{c.m.}}-V_B$, where V_B is the Coulomb-barrier height. (Here use is made of the values of V_B in Table IV, to be discussed in Sec. V C.) The open circles in Fig. 9 denote the values of th DR potential, while the solid circles are the values of the fusion potential. For the sake of comparison we present there also the values for the ^{6}He+^{209}Bi system [8].

It is remarkable that the values of the real and imaginary parts of the DR potential at R_{sa}, $V_D(R_{sa},E)$, and $W_D(R_{sa},E)$ are both considerably greater than those of the fusion potential, $V_F(R_{sa},E)$ and $W_F(R_{sa},E)$, respectively. This means that the total real and imaginary potentials at R_{sa} are dominated by the DR part, and thus the energy dependence of the summed potential is determined by that of the DR potential. This explains why the threshold anomaly was not seen in the potentials deduced in previous studies, unless they separated the optical potential into two parts [12,14,21].

B. Effects of breakup on fusion

There are two competing physical effects of breakup on fusion cross sections. The first is the lowering of the fusion barrier, which tends to enhance σ_F. The other is the removal of flux from the elastic into the breakup channel, which suppresses σ_F.

In the present treatment, these two competing effects are described in terms of the real $[V_D(r;E)]$ and the imaginary $[W_D(r;E)]$ parts of the DR potential. $V_D(r,E)$ can describe precisely the effect of lowering the barrier, while $W_D(r,E)$ represents the removal of the flux from the elastic channel. To see the effects quantitatively, we introduce the following factor R_i:

$$R_i = \sigma_F(i)/\sigma_F(V_D = W_D = 0) \quad (i = V, W, \text{or } VW), \quad (20)$$

where $\sigma_F(V_D=W_D=0)$ is σ_F obtained by setting $V_D=W_D=0$, i.e., neglecting both barrier-lowering and flux-loss effects,

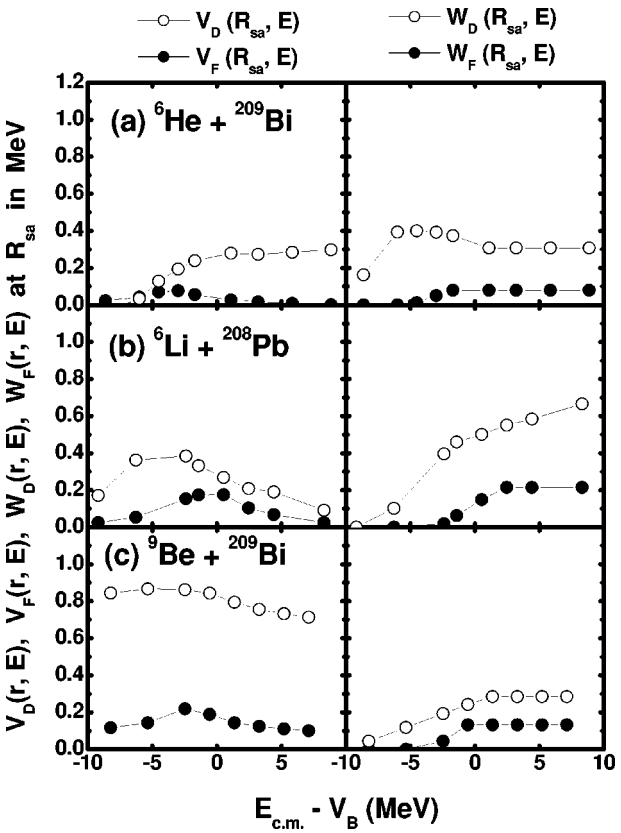

FIG. 9. The real (left panel) and imaginary (right panel) parts of fusion (solid circles) and DR (open circles) potentials as functions of $E_{\mathrm{c.m.}}-V_B$ at the strong absorption radius R_{sa} for (a) ^{6}He+^{209}Bi (R_{sa}=13.0 fm), (b) ^{6}Li+^{208}Pb (R_{sa}=11.9 fm), and (c) ^{9}B +^{209}Bi(R_{sa}=12.3 fm) systems. The lines connecting the circles are only to guide the eyes.

while $\sigma_F(i)$ is σ_F obtained by including either V_D (for $i=V$) or W_D (for $i=W$), or both (for $i=VW$). Thus R_V and R_W describe the barrier-lowering and flux-loss effects, respectively, while R_{VW} gives the net effect. Note that $\sigma_F(i=VW)$ is nothing but our final fusion cross section σ_F. The values of these ratios are summarized in Table III. As seen in Table III, R_V is always larger than unity, indicating that the barrier lowering enhances σ_F. On the other hand, R_W is smaller than unity, demonstrating that the flux loss suppresses σ_F.

In order to show the net effect clearly, we plot in Fig. 10 the R_{VW} values for the three systems considered in Table III, as functions of $E_{\mathrm{c.m.}}-V_B$. It is remarkable that R_{VW} shows an interesting projectile dependence; the curve for ^{9}Be has the largest R_{VW} values, that for ^{6}Li the next largest, and the curve for ^{6}He has the smallest values. It may be interesting to remark here that this order in the magnitudes of the ratio R_{VW} is related to the values of d_I, discussed earlier in Sec. II, that measure the strength of the breakup effect; the nuclear system with smaller d_I value has a larger R_{VW} value. In the higher-energy region, all R_{VW} values are smaller than unity, indicating that the flux-loss effect surpasses the barrier-lowering effect, resulting in the net suppression of σ_F.

Table III shows that the suppression factors R_{VW} at the highest energy for ^{6}He, ^{6}Li, and ^{9}Be are 0.76, 0.64, and 0.89, respectively. These values may be compared with the experimental values of R^{exp}=0.76, 0.59, and 0.92, respectively, which we deduce from

$$R^{exp}=\sigma_F^{exp}/\sigma_F^{cl}, \tag{21}$$

where σ_F^{cl} is the well-known BPM expression valid in the above-barrier energies,

$$\sigma_F^{cl}=\pi R_B^2\left(1-\frac{V_B}{E_{\mathrm{c.m.}}}\right). \tag{22}$$

Here R_B is the barrier radius, which we estimated by using the empirical formula of Vas, Alexander, and Satchler [4]. The values thus estimated are R_B=11.68, 10.34, and 11.48 fm, respectively, for the ^{6}He, ^{6}Li, and ^{9}Be cases. Thus, our calculated R_{VW} factors are very close to R^{exp}, indicating that the observed suppression in the above-barrier region can essentially be explained in terms of the net breakup effect.

TABLE III. $R_i=\sigma_F(i)/\sigma_F(V_D=W_D=0)$ for $i=V$, $i=W$, and $i=VW$.

System	$E_{\mathrm{c.m.}}$ (MeV)	$E_{\mathrm{c.m.}}-V_B$ (MeV)	R_V	R_W	R_{VW}
^{6}He+^{209}Bi	14.3	−6.0	1.03	0.92	0.94
	15.8	−4.5	1.13	0.84	0.93
	17.3	−3.0	1.24	0.73	0.88
	18.6	−1.7	1.26	0.68	0.83
	21.4	1.1	1.15	0.66	0.73
	23.5	3.2	1.08	0.68	0.76
	26.3	6.0	1.05	0.71	0.75
	29.2	8.9	1.04	0.73	0.76
^{6}Li+^{208}Pb	26.2	−2.4	1.33	0.77	1.03
	28.2	−1.4	1.34	0.78	1.02
	30.1	0.5	1.19	0.66	0.77
	32.1	2.5	1.08	0.64	0.69
	34.0	4.4	1.05	0.63	0.66
	37.9	8.3	1.01	0.63	0.64
^{9}Be+^{209}Bi	36.4	−2.5	2.30	0.90	2.01
	38.3	−0.6	1.78	0.83	1.43
	40.3	1.4	1.41	0.78	1.08
	42.2	3.3	1.22	0.78	0.95
	44.1	5.2	1.14	0.80	0.91
	46.0	7.1	1.09	0.81	0.89

C. Enhancement of σ_F in the subbarier region

Whether σ_F for loosely bound projectiles is enhanced or not in the subbarrier region is a subject of great current interest. We begin our discussion on this subject by defining a subbarrier enhancement factor Δ,

$$\Delta=V_B-E_{0,F}, \tag{23}$$

where $E_{0,F}$ is the subbarrier threshold energy introduced by Stelson *et al.* [39] [see also Eq. (15)] and V_B is the Coulomb-barrier height. Δ is a measure of how far below the barrier

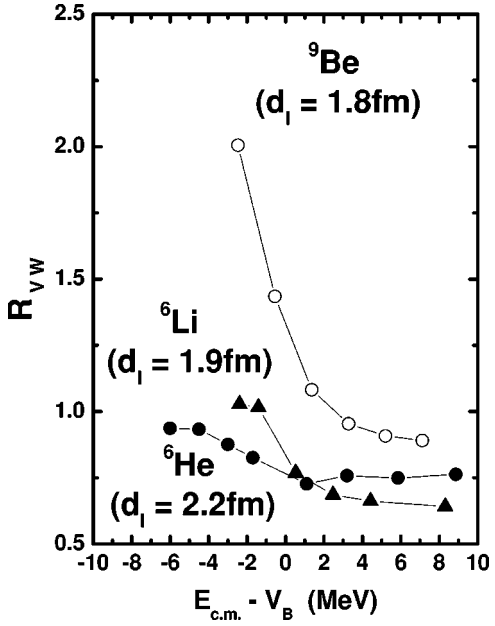

FIG. 10. The calculated ratios $R_{VW}=\sigma_F(VW)/\sigma_F(V_D=W_D=0)$ with $\sigma_F(V_D=W_D=0)$ calculated by setting $V_D(E)=W_D(E)=0$, $\sigma_F(VW)$ calculated by including both $V_D(E)$ and $W_D(E)$, thus describing the net breakup (DR) effect, are shown as functions of $E_{\text{c.m.}}-V_B$ for ^{6}He+^{209}Bi, ^{6}Li+^{208}Pb, and ^{9}Be+^{209}Bi systems.

fusion can still take place, and thus we refer to it as a subbarrier enhancement factor. Since both $E_{0,F}$ and V_B can be extracted from the measured fusion cross-section data by using Eqs. (15) and (22), respectively, Δ provides a model-independent measure of the subbarrier enhancement.

Table IV summarizes the values of Δ, together with V_B, $E_{0,F}$ and also "x number of neutron" transfer threshold energy Q_{xn}. These values are listed not only for the three systems considered here, but also for the ^{4}He+^{209}Bi and ^{11}Be +^{209}Bi systems. Restricting our interests to the first three projectile cases, we see that ^{6}He has the largest Δ, ^{9}Be the next, and ^{6}Li the smallest Δ. This contradicts what is expected from the calculated R_{VW} values, which predicts that σ_F for ^{6}He should be suppressed there. This indicates that the observed enhancement for ^{6}He cannot be explained in terms of breakup effects, suggesting that breakup is not the primary mechanism that governs subbarrier fusion.

We recall at this stage that an alternative mechanism has been proposed by Stelson *et al.* [39]; according to the authors, the subbarrier fusion starts to occur when the colliding nuclei come within a distance where the barrier against valence neutron flow disappears and thus the flow takes place freely. This means that subbarrier fusion will be more enhanced if a collision system has a larger positive neutron(s) transfer Q value [or equivalently if a projectile has less neutron(s) binding energy].

TABLE IV. Subbarrier enhancement factors. Uncertainties in the V_B and $E_{0,F}$ values listed here are expected to be only a few percent, but those in the Δ values may amount to as large as 10%, since Δ is determined as a difference between V_B and $E_{0,F}$.

System	$E_{0,F}$ (MeV)	V_B (MeV)	Δ (MeV)	Q_{xn}	x
^{6}He+^{209}Bi	15.4	20.3	4.9	8.77	2
^{9}Be+^{209}Bi	35.5	38.9	3.4	2.94	1
^{6}Li+^{208}Pb	26.8	29.6	2.8	−1.73	1
^{11}Be+^{209}Bi	36.2	39.6	3.4	4.10	1
^{4}He+^{209}Bi	18.2	20.2	2.0	−8.35	1

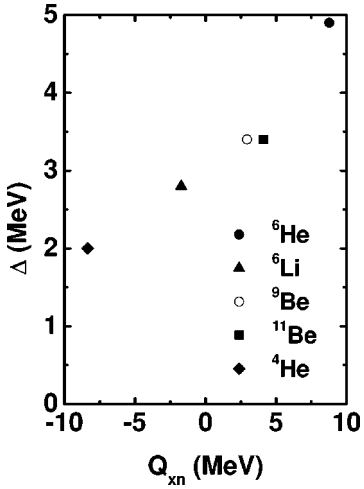

FIG. 11. The experimental values of the subbarrier enhancement factor Δ as a function of the neutron(s) transfer Q value.

In Fig. 11, we present the values Δ as a function of Q_{xn}, where $x=1$ for all cases except ^{6}He with $x=2$. As seen, Δ has a strong correlation with Q_{xn}, supporting the idea of Stelson *et al.* It should be noted that a similar argument supporting the idea of Stelson *et al.* has been given by Kolata *et al.* [11] who took the data for ^{6}He, and also very recently by Zagrebaev [40].

Finally, we note that this mechanism of enhancement due to neutron transfer is phenomenologically implemented in the present description through the parameters of the fusion potentials, specifically by the strength parameters $W_F(E)$ of $W_F(r;E)$.

D. Effects of the DR and fusion potentials on elastic scattering cross sections

So far, we have concentrated on the breakup effects on the fusion cross section. It may also be interesting to see the effect on the elastic scattering cross section. In Fig. 12 we illustrate the effect, taking, as an example, the case for ^{9}Be +^{209}Bi at $E_{lab}=46$ MeV. Plotted in Fig. 12 are the calculated P_E obtained by setting $V_D=0$ or $W_D=0$, or $V_D=W_D=0$ in comparison with the P_E from the full calculation. As seen, if one neglects either V_D or W_D, or both, P_E changes, but mostly in the region of $d=d_{sa}\sim d_I$. This is understandable, since it is the region where DR takes place and thus the DR potential is most influential in that region. It is remarkable that once the DR potential is neglected, the interaction distance of the resultant P_E is reduced to $d_I\approx 1.65$, close to the value for the normal tightly bound projectiles.

We have further studied the effects of the fusion potential on the elastic-scattering cross section, particularly focusing

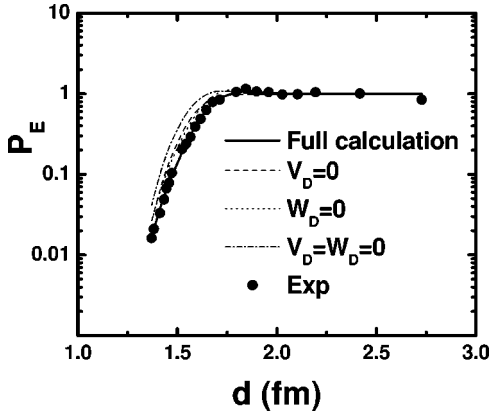

FIG. 12. Effects of the DR potential on P_E for the ^{9}Be+^{209}Bi system at E_{lab}=46 MeV. P_E calculated by setting $V_D(E)=0$ (dashed line), $W_D=0$ (dotted line), and $V_D(E)=W_D=0$ (dash-dotted line) are compared with P_E, including both V_D and W_D (solid curve).

on the fusion radius parameter, r_F. Presented in Fig. 13(a) is a plot of the χ^2 values as a function of r_F, calculated by using the same parameters as used for the final cross-section calculation excepting r_F. As seen, the χ^2 value has a well established minimum at $r_F=1.40$ fm. To see the variations in P_E values when they are calculated with r_F values different from the best fit value of $r_F=1.40$ fm, we plot in Fig. 13(b) P_E for three cases of $r_F=1.35$, 1.40, and 1.45 fm in comparison with the data. As seen, if one changes the r_F value from the best fit value, the fit to the data gets deteriorated, particularly in the region of $d<d_{sa}\approx 1.55$ fm, where fusion is supposed to take place strongly.

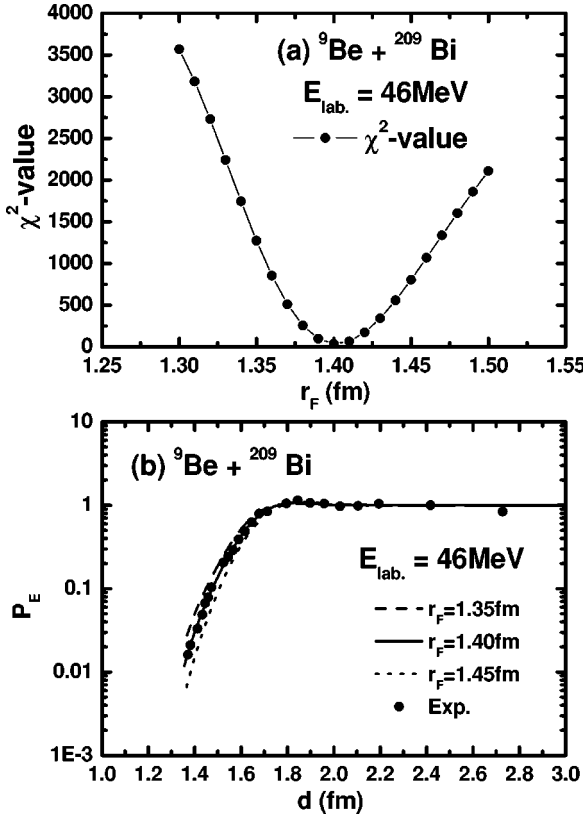

FIG. 13. (a) The χ^2 values as a function of r_F evaluated for 1.30 fm$<r_F<$1.50 fm and (b) P_E as a function of d evaluated with $r_F=1.35$, 1.40, and 1.45 fm for the ^{9}Be+^{209}Bi system at E_{lab} =46 MeV.

VI. CONCLUSIONS

In summary, we have carried out simultaneous χ^2 analyses of elastic scattering, DR (breakup), and fusion cross sections for the ^{6}Li+^{208}Pb and ^{9}Be+^{209}Bi systems at near-Coulomb-barrier energies within the framework of an extended optical model that introduces two types of complex polarization potentials: the DR and fusion potentials. The results show that the extracted potentials satisfy the dispersion relation well and that the fusion potential exhibits a threshold anomaly very similar to that observed for tightly bound projectiles. The results also show that at the strong absorption radius, the magnitudes of the fusion potential are much smaller than those of the DR potential. As a consequence, the resulting total polarization potential becomes rather a smooth function of the incident energy, similar to that of the DR potential. This explains why the threshold anomaly has not been observed in potentials determined without separating the fusion part from the DR part.

Using the extracted DR potentials, studies were made of the breakup (DR) effects on the fusion cross section σ_F. The effects are found to be strongly projectile-dependent, reflecting the significance of the probability of breakup of the projectile. It is also argued that breakup is not the main cause of the subbarrier enhancement of the fusion cross section, but that the mechanism that governs the enhancement is neutron flow as originally suggested by Stelson *et al.* [39]. In the present description, this effect is phenomenologically implemented in the imaginary part of the fusion potential. We also find that the experimental suppression factors for σ_F in the above-barrier region are 0.76, 0.59, and 0.92 for ^{6}He, ^{6}Li, and ^{9}Be, respectively, which are in fairly good agreement with theoretical suppression factors of 0.76, 0.64, and 0.89, respectively.

ACKNOWLEDGMENTS

The authors sincerely thank Dr. N. Keeley, Dr. C. Signorini, Dr. R. P. Ward, Dr. N. M. Clarke, and Dr. C. J. Lin for kindly sending the numerical tables of their data. The authors also wish to express sincere thanks to Professor W. R. Coker for kindly reading the manuscript and comments. The work was supported by the Basic Research Program of the KOSEF, Korea (Grant No. R05-2003-000-12088-0).

[1] T. Udagawa, B. T. Kim, and T. Tamura, Phys. Rev. C **32**, 124 (1985); T. Udagawa and T. Tamura, *ibid.* **29**, 1922 (1984).
[2] S.-W. Hong, T. Udagawa, and T. Tamura, Nucl. Phys. **A491**, 492 (1989).
[3] T. Udagawa, T. Tamura, and B. T. Kim, Phys. Rev. C **39**, 1840 (1989); B. T. Kim, M. Naito, and T. Udagawa, Phys. Lett. B **237**, 19 (1990).
[4] L. C. Vas, J. M. Alexander, and G. R. Satchler, Phys. Rep. **69**, 373 (1981).
[5] C. H. Dasso, S. Landowne, and A. Winther, Nucl. Phys. **A407**, 221 (1983).
[6] G. R. Satchler, *Introduction to Nuclear Reactions* (Wiley, New York, 1980).
[7] B. T. Kim, W. Y. So, S. W. Hong, and T. Udagawa, Phys. Rev. C **65**, 044607 (2002).
[8] B. T. Kim, W. Y. So, S. W. Hong, and T. Udagawa, Phys. Rev. C **65**, 044616 (2002).
[9] C. C. Mahaux, H. Ngo, and G. R. Satchler, Nucl. Phys. **A449**, 354 (1986); **A456**, 134 (1986).
[10] M. A. Nagarajan, C. C. Mahaux, and G. R. Satchler, Phys. Rev. Lett. **54**, 1136 (1985).
[11] J. J. Kolata *et al.*, Phys. Rev. Lett. **81**, 4580 (1998).
[12] E. F. Aguilera *et al.*, Phys. Rev. Lett. **84**, 5058 (2000).
[13] E. F. Aguilera *et al.*, Phys. Rev. C **63**, 061603(R) (2001).
[14] N. Keeley, S. J. Bennett, N. M. Clarke, B. R. Fulton, G. Tungate, P. V. Drumm, M. A. Nagarajan, and J. S. Lilly, Nucl. Phys. **A571**, 326 (1994).
[15] G. R. Kelly *et al.*, Phys. Rev. C **63**, 024601 (2001).
[16] C. Signorini *et al.*, Eur. Phys. J. A **10**, 249 (2001).
[17] M. Mazzocco *et al.*, in *Proceedings of the International Conference*, Lipari, Italy, 2001, edited by Y. Yidrdino *et al.* (World Scientific, Singapore, 2002).
[18] C. Signorini *et al.*, Phys. Rev. C **67**, 044607 (2003).
[19] M. Dasgupta *et al.*, Phys. Rev. C **66**, 041602(R) (2002).
[20] Y. W. Wu, Z. H. Liu, C. J. Lin, H. Q. Zhang, M. Ruan, F. Yang, and Z. C. Li, Phys. Rev. C **68**, 044605 (2003).
[21] C. Signorini *et al.*, Eur. Phys. J. A **5**, 7 (1999); (private communication).
[22] M. Dasgupta *et al.*, Phys. Rev. Lett. **82**, 1395 (1999).
[23] C. Signorini *et al.*, Phys. Rev. C **61**, 061603(R) (2000).
[24] C. Signorini *et al.*, in *Proceedings of the International Conference BO2000*, edited by D. Vretenar (World Scientific, Singapore, 2001).
[25] C. Signorini, Nucl. Phys. **A693**, 190 (2001).
[26] C. Signorini, Eur. Phys. J. A **13**, 129 (2002).
[27] D. J. Hinde, M. Dasgupta, B. R. Fulton, C. R. Morton, R. J. Wooliscroft, A. C. Berriman, and K. Hagino, Phys. Rev. Lett. **89**, 272701 (2002).
[28] R. J. Woolliscroft, N. M. Clarke, B. R. Fulton, R. L. Cowin, M. Dasgupta, D. J. Hinde, C. R. Morton, and A. C. Berriman, Phys. Rev. C **68**, 014611 (2003).
[29] T. Udagawa, M. Naito, and B. T. Kim, Phys. Rev. C **45**, 876 (1992).
[30] R. Bass, *Nuclear Reactions with Heavy Ions* (Springer-Verlag, New York, 1980).
[31] J. T. Holdeman and R. M. Thaler, Phys. Rev. **139**, B1186 (1965).
[32] H. Wojciechowski, D. E. Gustafson, L. R. Medsker, and R. H. Davis, Phys. Lett. **63B**, 413 (1976).
[33] H. Wojciechowski, L. R. Medsker, and R. H. Davis, Phys. Rev. C **16**, 1767 (1977).
[34] P. R. Christensen, V. I. Manko, F. D. Becchetti, and R. J. Nickles, Nucl. Phys. **A207**, 33 (1973).
[35] R. A. Broglia and A. Winther, *Heavy Ion Reactions Lecture Note Volume I: Elastic and Inelastic Reactions* (Benjamins, London, 1981), p. 165.
[36] W. G. Love, T. Terasawa, and G. R. Satchler, Nucl. Phys. **291**, 183 (1977).
[37] G. R. Satchler and W. G. Love, Phys. Rep. **55**, 183 (1979).
[38] M. S. Hussein, Phys. Rev. C **30**, 1962 (1984).
[39] P. H. Stelson, Phys. Lett. B **205**, 190 (1988); P. H. Stelson, H. J. Kim, M. Beckerman, D. Shapira, and R. L. Robinson, Phys. Rev. C **41**, 1584 (1990).
[40] V. I. Zagrebaev, Phys. Rev. C **67**, 061601(R) (2003).